HHS Public Access

Author manuscript

Mol Cancer Res. Author manuscript; available in PMC 2024 November 02.

Published in final edited form as:

Mol Cancer Res. 2024 May 02; 22(5): 440–451. doi:10.1158/1541-7786.MCR-23-0199.

Oncogenic GNAS uses PKA-dependent and independent mechanisms to induce cell proliferation in human pancreatic ductal and acinar organoids

Ridhdhi Desai[1,2], **Ling Huang**[1,3], **Raul S. Gonzalez**[1], **Senthil K. Muthuswamy**[4,*]

[1]Cancer Research Institute, Department of Medicine, Beth Israel Deaconess Medical Center, Harvard Medical School, Boston, MA 02215, USA

[2]*Current Address:* Islet Cell and Regenerative Biology, Joslin Diabetes Center, Harvard Medical School, Boston, MA, USA.

[3]*Current Address:* Department of Surgery, Henry Ford Pancreatic Cancer Center, Henry Ford Health, Detroit, Michigan

[4]*Laboratory* of Cancer Biology and Genetics, National Cancer Institute, NIH, Bethesda, MD, MA, 02215, USA

Abstract

Ductal and acinar pancreatic organoids are promising models for the study of pancreatic diseases. Genome sequencing studies have revealed that mutations in a G-protein (*GNAS*^{R201C}) are exclusively observed in intraductal papillary mucinous neoplasms (IPMNs). The biological mechanisms by which GNAS^{R201C} affects the ductal and acinar exocrine pancreas are unclear. Here, we use human stem-cell-derived pancreatic ductal and acinar organoids and demonstrate that GNAS^{R201C} was more effective in inducing proliferation in ductal organoids compared to acinar organoids. Surprisingly, GNAS^{R201C}-induced cell proliferation was protein kinase A (PKA)-independent in ductal organoids and an immortalized ductal epithelial cell line. Co-expression of oncogenic *KRASG12V* and *GNAS*^{R201C} retained PKA-independence in ductal organoids to stimulate cell proliferation. Thus, we identify cell lineage-specific roles for PKA signaling in GNAS^{R201C}-driven cell proliferation in pre-cancerous lesions and report the development of a human pancreatic ductal organoid model system to investigate mechanisms regulating GNAS^{R201C}-induced IPMNs.

Implications: The study identifies an opportunity to discover a PKA-independent pathway downstream of oncogene GNAS for managing IPMN lesions and their progression to PDAC

*Corresponding author: senthil.muthuswamy@nih.gov phone: (240) 858-7734.

Authors contributions

Conception and design: R. Desai and S. Muthuswamy

Development of methodology: R. Desai and S. Muthuswamy

Acquisition of data: R. Desai, Ling Huang, Raul Gonzalez (analyzed the histopathology of pancreatic transplants)

Analysis and Interpretations of data: R. Desai and S. Muthuswamy

Writing, review, and/or revision of manuscript: R. Desai and S. Muthuswamy

Study supervision: R. Desai and S. Muthuswamy

Authors' Disclosures

No potential conflicts of interest were disclosed

Introduction

In the pancreas, IPMNs are the most common pancreatic cystic neoplasms and are characterized as large, mucinous cystic structures that can be clinically diagnosed through abdominal imaging (1,2). Genomic analysis using whole exome and next-generation sequencing of IPMN patient samples indicate that mutations in oncogenes *KRAS*$^{G12V/D}$, and *GNAS*^{R201C} occur early during IPMN development (3,1,4,5,6). Here, activating mutations of *KRAS* (G12D or G12V) are found in ~80% of cases, while activating mutations of *GNAS* (R201C or R201H) are observed in 66% of IPMN patients, respectively (4,5,6). In particular, unlike *KRAS*, *GNAS* mutations are exclusively observed in IPMNs, underscoring the importance of their function in IPMN development. It is not clear if the expression of GNAS mutation is sufficient to induce disease phenotypes. Genetically engineered mouse models (GEMMs) indicate that co-expression of GNAS^{R201C} and oncogenic KRAS^{G12D} under the control of pdx1 or ptf1a promoters can form cystic, IPMN-like lesions (7,8,9). Pdx1- or Ptf1a promoters drives the expression of the transgenes in embryonic pancreatic precursors in these GEMM models, leading to genetic changes in both ductal and acinar cell lineages. Thus, how mutant GNAS functions in the acinar or ductal lineages of the exocrine compartments to regulate the initiation and progression of IPMN lesions is poorly understood.

GNAS encodes the stimulatory subunit of a heterotrimeric G-protein, Gαs, that is involved in G-protein-coupled receptor (GPCR) signaling. Under homeostatic conditions, ligand-based activation of GPCRs promotes an exchange of GDP for GTP on Gαs. GTP-bound Gαs then activates adenylate cyclase and increases cytoplasmic levels of cyclic adenosine monophosphate (cAMP) (10,11,12). *GNAS*^{R201C} mutations maintain Gαs in an active GTP-bound state and increase cAMP levels, which upregulates protein kinase A (PKA) and other downstream signaling cascades, including cyclin nucleotide-gated ion channels and EPAC1/2 guanine-nucleotide exchange factors. Activating mutations of *GNAS* were first described in endocrine neoplasms, particularly pituitary adenomas (13,14). Since then, they have been identified to promote aberrant growth and proliferation in small cell lung cancer and gastrointestinal cancers, including colon, gastric carcinoma, and intraductal papillary mucinous neoplasms (IPMN) (15,16,17,18,19).

We have previously developed pancreatic ductal and acinar organoid models from human embryonic stem cell-derived pancreatic progenitor cells and used them to model pancreatic dysplasia *in vitro* and pancreatic cancer progression *in vivo* (20). We reported that oncogenic GNAS induces IPMN-associated phenotypes, including lumen dilation and Muc2 production, specifically in the ductal but not acinar organoids (20), identifying the utility of the platform to investigate lineage-specific biological mechanisms.

Here, we investigate the role played by PKA signaling in regulating oncogenic GNAS-induced effects on the exocrine pancreas. GNAS^{R201C}-mediated activation of PKA-signaling induced the formation of Muc2-expressing cystic structures in ductal organoids; however, GNAS-induced cell proliferation was independent of the PKA signaling pathway using two independent PKA inhibitors. Interestingly, unlike ductal organoids, GNASR201C-induced cell proliferation in acinar organoids was PKA-dependent, demonstrating that

GNAS^{R201C} uses lineage-specific mechanisms to promote proliferation in the pancreatic exocrine lineage. Co-expression of *GNAS* and *KRAS* (*R201C/G12V*) neither augmented nor altered PKA independence in ductal organoids. In addition, we report the establishment of long-term cultures of *GNAS^{R201C}*-expressing pancreatic ductal organoids from pancreatic progenitors to serve as a platform for investigating mechanisms by which GNAS promotes proliferation in a PKA-independent manner. In summary, we demonstrate a lineage-specific role for PKA signaling in regulating oncogene GNAS-induced cell proliferation and demonstrate the utility of stem cell-derived organoid models for investigating cell lineage-specific mechanisms regulating pancreatic cancer initiation.

Materials and Methods

Cell lines, Cell culture, and Animal models

Embryonic Pluripotent stem cells: In this study, HUESC8 stem cells were differentiated towards the pancreatic progenitors stage in the lab of Dr. Douglas Melton, Harvard University, using previously described protocols (20,21,22).

HPDE cells: HPDE cell line was obtained from Dr. Ming Tsao (University of Toronto). The cell line was not independently re-authenticated upon receipt. They were maintained in DMEM-HG (Gibco) supplemented with inactivated FBS and antibiotics at 37°C in 5% CO_2. Stable HPDE cell lines expressing *GNAS^{WT}* or *GNAS^{R201C}* were established using lentiviral transduction. The cell lines were routinely screened for Mycoplasma every two months using the Lonza MycoAlert Mycoplasma Detection kit (Cat# LT07–318). To culture cells expressing the transgenes in 3D, 8-well falcon chamber slides were coated with ~15μl of 100% Matrigel (Growth factor reduced, Corning) and incubated at 37°C for 30 minutes to polymerize. ~40,000 cells were seeded in each coated well in media containing 2% Matrigel. On Day 4, 1μg/ml doxycycline, with or without H89 (10μM or otherwise as indicated) was added in fresh media to induce gene expression, and cell viability was measured using cell titer glow 3D using manufacturer's instructions (Promega) on Day7 and Day10. Culture media was replaced with fresh media on Day 7 with doxycycline. Experiments were performed within the first ten passages after thawing.

Animal models: Six-eight-week-old male immunodeficient NCG (NOD CRISPR *Prkdc Il2r* Gamma) mice were purchased from Charles River (Catalog #572) and used for orthotopic transplantation experiments. All animal experiments were approved by IACUC committee at Beth Israel Deaconess Medical Center (Boston, MA).

Induction and culture of ductal and acinar organoids

Ductal and acinar organoid induction from pancreatic progenitors was performed as previously described (20). Cell culture plates or 8-well falcon chamber slides were coated with undiluted Matrigel (~100μl for each well of an 8-well chamber slide or ~500μl for each well of a 6-well plate) and incubated at 37°C to solidify. Transduced or uninfected pancreatic progenitors were seeded as single cells on Matrigel-coated plates in appropriate differentiation media (described in 20) containing 5% Matrigel. Media change was performed every 4 days. For long-term culture of *GNAS^{R201C}*-expressing organoids,

Day16 ductal organoids were digested using 1.0 mg/ml Collagenase/Dispase (Sigma) in DMEM-HG (Gibco) for 30 – 60minutes, followed by mechanical dissociation of organoids using a p1000 pipette. After centrifugation (1000rpm, 5min), dissociated organoids were embedded in 100% Matrigel and seeded at 1:3 split ratio as 80µl domes in 24-well cell culture plates. The domes were allowed to solidify for 30 minutes at 37°C. Stage 4 ductal differentiation media containing doxycycline (1.0 µg/ml) was used to culture and maintain the growth of *GNAS*^{R201C}-expressing ductal organoids. Culture media was replaced every four days and organoids were split in a 1:3 ratio every 12–16 days.

Chemicals, Drugs, and Antibodies

All reagents used for ductal and acinar organoids are previously described (20). Forskolin (1099), KT-5720 (1288), and 8-CpT-0-Me-cAMP (1645) were from Tocris. H89 (S1582) was from Selleckchem; 8-Br-cAMP (B7880) was from Sigma.

The following antibodies were used: GNAS (371732, Millipore, RRID:AB_10680769), GFP (632381,JL-8, Takara Bio, RRID:AB_2313808), p-VASP (3111, cell signaling, RRID:AB_331569), T-VASP (3132, cell signaling, RRID:AB_2213393), pPKA substrate (9624, cell signaling, RRID:AB_331817), Vinculin (13901, cell signaling, RRID:AB_2728768).

Plasmids and Cloning

All oncogenes were cloned into pInducer10 (addgene). *GNAS*^{R201C} (plasmid kindly provided by Dr. Anirban Maitra) was generated as previously described (20)

To generate pINGFPKRASG12V vector, GFP-tagged *KRAS(G12V)* was amplified by PCR from pQCXIPGFPKRASG12V using primers that contain Age1 and Not1 at the N- and C-terminus: Forward, 5'-ACCGGTCGCCACCATGGTGAGCAAGGGCGAGG-3'; Reverse, 5'-GCGGCCGC TTACATAATTAC-3', the PCR products were then subcloned into pINducer10 using Age1 and Not1.

To generate pINR201C/G12V vector, GNAS^{R201C} was amplified using a forward primer containing Age1 and a reverse primer containing P2A sequence followed by a Not1 restriction site: Forward, 5'- 5'ACC GGT CGC CAC CAT GGG3'; Reverse, 5'-GCGGCCGCCTCCGGGACCGGGGTTTTCTTCCACGTCTCCTGCTTGCTTTAACAGA GAGAAGTTCGTGGCTCCGGAGCCGAGCAGCTCGTACTGACG3'. Both PCR products were then subcloned into pINducer10 using Age1 and Not1. All final plasmids were sequence verified.

Virus production and infection

Lentiviruses were produced in 293T cells using packaging plasmids (pCMV-dR8.9 and pMD2.G). Viral particles were concentrated using Lentivirus precipitation solution (ALSTEM). Viral pellets were resuspended in PBS and frozen as aliquots at −80°C.

To infect HPDE cells, 150,000 cells were seeded per well of a 6-well plate. Concentrated lentiviral particles were added to the cells and spinfected at 2250 rpm for 30 minutes. The viral media was then discarded. The cells were washed once with PBS, and fresh culture

media was added. Cells expressing the transgene were selected 48 hours after infection with 2.0 μg/ml puromycin.

To infect pancreatic progenitors, 48-well plates were first coated with 5% Matrigel for ~2–3 hours. At the time of seeding, the Matrigel solution was aspirated, and the plates were allowed to air dry. ~150,000 single pancreatic progenitor cells were then seeded as a monolayer in each Matrigel-coated well. After 24 hours, lentiviruses supplemented with 4.0 μg/ml polybrene were added to each well, and the plates were incubated at 37°C overnight. The next day, infected cells were briefly digested with Accutase (Sigma) and centrifuged at 1500 rpm for 5 minutes. The pellet was resuspended in either ductal or acinar stage 1 differentiation media, and ~40,000 cells were seeded per well of an 8-well chamber slide. 0.3 μg/ml of puromycin was added on Day 3 post-seeding to select for transgene-expressing cells. 1.0 μg/ml of doxycycline was added to the culture media to induce transgene expression at indicated time points.

Orthotopic transplantations in mouse pancreas

Day16 ductal and acinar organoids expressing either *KRAS(G12V)* or *R201C/G12V* were dissociated using collagenase/Dispase (Roche) for 2 hours followed by 30 minutes of dissociation by Accutase (Sigma). Dissociated single cells were counted and approximately 500,000 cells were resuspended in 50μl of 50% Matrigel. Orthotopic transplantations were conducted as previously described in (20) in NCG mice (#572, Charles River). Mice were fed with a doxycycline-containing diet for 8–14 weeks post-transplantation, after which they were sacrificed. Extracted pancreas were then processed to generate paraffin blocks.

Phase contrast image analysis

For phase contrast imaging, at least 50–100 organoid images (per experiment) were taken using either a 4X or a 10X objective. Image Analysis was performed using ImageJ. Briefly, the longest diameter (d) of each organoid was measured, and the area was calculated as $\pi(d/2)^2$.

Click-it EdU proliferation assay and Immunofluorescence

For Edu proliferation assays, ductal and acinar organoids were incubated with 10 μM Edu for 4 hours at 37°C in an incubator. Both ductal and acinar structures were fixed in 4%PFA in PBS for 30 minutes at RT and then processed for Edu-Click-iT according to the manufacturer's instructions (Thermo Fisher). For immunofluorescence stainings, fixed organoids were first incubated with immunofluorescence buffer (7 mM sodium dibasic heptahydrate, 3 mM sodium monobasic monohydrate, 131 mM NaCl, 0.1% BSA, 0.02% Tween 20, and 0.2% Triton X-100) for 15–30 min at RT. Organoids were then blocked with 0.5% Triton X-100 and 1% BSA for 15–30 min at RT followed by incubation with primary antibody (in PBS with 1%BSA) overnight at 4°C. Organoids were washed with PBS 3X for 10 min and then incubated with secondary antibody (in PBS with 1% BSA) and DAPI to mark the nuclei for 1hr at room temperature. Confocal images of the mid-section of each organoid were taken on a Zeiss LSM880 inverted live-cell microscope. Images were processed using Zeiss Zen, and ImageJ was used to determine the percentage of Edu^{+ve} cells at the mid-section of each organoid.

Protein Analysis and Western Blotting

For western blotting, ductal and acinar cells were collected in 15 ml falcon tubes by resuspension in ice-cold PBS. The suspension was centrifuged at 3500 rpm for 5 minutes. The resulting pellet was then resuspended in ice-cold cell recovery media and incubated for 30 minutes at 4C. The tubes were then centrifuged at 3500rpm for 5 minutes. The supernatant was discarded, and the pellet was washed with ice-cold PBS, followed by centrifugation at 3500 rpm for 5 minutes. The resulting pellets were lysed in RIPA buffer supplemented with phosphatase and protease inhibitors (Roche). Protein concentration was determined by Bradford assay, and standard procedures were used for western blotting. Primary antibodies used for western analysis: pPKA substrates (1:1000), pVASP (1:500), T-VASP (1:500), Vinculin (1:10000), GNAS (1:1000), GAPDH (1:2000).

RNA extraction and qPCR analysis

Organoids were first washed once with cold PBS. Fresh cold RLT buffer from an RNA isolation kit (Qiagen – RNeasy plant mini kit, Cat#74904) was added directly to the plates containing organoids. The organoids were scraped using a cell scraper, and the slurry was collected in a clean falcon tube. Purified RNA was isolated using the protocol from the RNeasy Plant Mini Kit (Cat#74904). cDNA was generated using qScript cDNA Synthesis Kit (Quanta Biosciences – Cat # 95047–025). Gene expression was quantitated by quantitative PCR using the PrimeTime qPCR Probe Assays kit. The following previously described Taqman Probes (IDT) were used – Sox9 -Hs.PT.58.38984663; Ptf1a-Hs.PT.58.45382933.g; Nkx6.1 – Hs.PT.58.25073618 (20)

Statistics and Reproducibility

For most experiments, data was collected from at least 3 independent (i.e. three independently transduced differentiations) experiments. All quantitative data are expressed as mean ± s.e.m unless indicated otherwise. Statistical differences were assayed by using a two-tailed student t-test using Prism 5 (GraphPad software). All quantitative data were collected from experiments performed in at least three samples or biological replicates. Significant differences are defined as follows: * $P<0.05$, ** $P<0.01$, *** $P<0.001$, **** $P<0.0001$.

Data Availability

All the data that support the findings of this study are available upon request from the corresponding author.

Results

Oncogenic $GNAS^{R201C}$ promotes the proliferation of ductal organoids in a PKA-independent manner

We previously showed that pancreatic progenitors can be differentiated into ductal-like and acinar-like organoids where they display increased levels of ductal (Sox9, CAII) and acinar (Ptf1a, CPA1) markers, respectively (20). To confirm that the organoids used in the present study express lineage-specific markers, we analyzed the expression of ductal and acinar

markers and demonstrated that acinar and ductal organoids retain lineage-specific marker expression (Fig. 1A; Supplementary Fig. S1A). We also showed that the expression of oncogenic *GNAS(R201C)* in HuESC-derived ductal, but not in acinar organoids, induced lumen dilation, recapitulating important features of IPMN lesions (Fig. 1B). To begin to understand the mechanism by which GNAS functions in these cell types, we investigated the role played by the PKA signaling pathway. $GNAS^{R201C}$ expression induced activation PKA signaling equally in both ductal and acinar lineages as monitored by total levels of phosphorylated PKA (pPKA) substrates and phosphorylation of a specific PKA substrate vasodilator-stimulated phosphoprotein (VASP) (Supplementary Fig. S1B and S1C). The treatment of H89, a PKA inhibitor, decreased pPKA and pVASP in GNAS-expressing ductal organoids (Fig. 1C), demonstrating inhibition of PKA activity. On day 8, organoids were treated with H89 and doxycycline to induce R201C expression and were analyzed on Day 16. Although the ability of R201C to induce lumen formation was not impaired by H89 treatment, in R201C-activated ductal structures, H89 treatment resulted in a significant decrease in lumen expansion, and Muc2 production (Fig. 1D, 1E, 1F).

Oncogenic GNAS induced a significant increase in total cell numbers, as measured by an increase in both the total number of nuclei per ductal organoid and viable cells (Fig. 2A, 2B). Here, inhibition of PKA signaling did not significantly alter the R201C-induced increase in viable cells of ductal organoids (Fig. 2B). Activation of R201C in ductal organoids induced EdU incorporation in ~10% of the cells with a ~6-fold increase in the percentage of EdU^{+ve} cells (Fig. 2C). Whereas in acinar organoids R201C activation induced EdU incorporation in ~2% of the cells with a ~4.0 fold increase in the percentage of EdU^{+ve} cells (Fig. 2C). Approximately 60% of R201C-expressing ductal organoids contained two or more EdU^{+ve} cells (Fig. 2D) both in the absence and presence of H89, suggesting a PKA-independent mechanism for promoting cell proliferation. By contrast, only 3% of R201C-expressing acinar organoids contained two or more EdU^{+ve} cells, which was inhibited by H89 (Fig. 2D).

To demonstrate that the PKA-independent proliferation is not restricted to stem cell-derived organoids, we evaluated R201C-induced proliferation in an immortalized human pancreatic ductal epithelial (HPDE) cell line that was engineered to overexpress wild-type (WT) or R201C mutant GNAS (Fig. 2E). When cultured in 3D, expression of WT *GNAS* (*GNAS*) showed a ~3.1-fold increase in viable cells three days post doxycycline and a 1.7X increase at six days post doxycycline (Fig. 2F). In comparison, R201C-expression promoted a ~3.44-fold increase in viable cells three days post Dox stimulation and a ~4.68-fold increase at six days post dox stimulation (Fig. 2F). Consistent with the results obtained using stem cell-derived organoids, H89-inhibited PKA signaling, as monitored by immunoblot analysis (Fig. 2G), and did not significantly alter R201C-induced proliferation in HPDE cells (Fig. 2F). Interestingly, R201C failed to induce proliferation of HPDE cells grown as monolayer cultures (Fig. 2H), suggesting a role for the 3D microenvironment for R201C-induced cell proliferation of HPDE cells. Together, our findings demonstrate that oncogenic GNAS induces cell proliferation independent of the PKA signaling pathway in the ductal cell lineage of the exocrine pancreas.

Coexpression of oncogenic *GNAS* and *KRAS* do not enhance the proliferation effects in ductal and acinar organoids

In addition to GNAS mutations, mutations in KRAS are frequently found in cystic lesions of the pancreas and have been shown to co-occur in ~50% of IPMN lesions (4). To address the cooperative effect between GNAS and KRAS in our stem cell model, we investigated whether oncogenic KRAS can modulate R201C-associated phenotypes in ductal and acinar structures. We generated dox-inducible lentiviral plasmids that co-express mutant forms of *GNAS(R201C)* and GFP-tagged *KRAS(G12V)* (denoted hereafter as *R201C/G12V*) using bicistronic expression systems (P2A peptides) (Fig. 3A). As expected, oncogenic KRAS is normally localized to the cell membrane in both *G12V* and *R201C/G12V*-expressing organoids (Fig. 3B). *KRASG12V* expression did not induce a detectable increase in pVASP or pPKA substrates in ductal organoids, whereas it induced an increase in PKA signaling in acinar organoids (Fig. 3C, 3D). Coactivation of both oncogenic KRAS(G12V) and GNAS(R201C) increased pVASP in both lineages; however, the pVASP levels were greater in acinar organoids compared to ductal organoids (Fig. 3C, 3D).

Co-expression of *R201C/G12V* increased the proliferation of ductal structures, as measured using EdU incorporation, albeit at a slightly lower rate than R201C-expressing ductal organoids (31 Vs 21 fold) (Fig. 3E). Interestingly, inhibition of PKA signaling using a PKA inhibitor (H89) did not attenuate the cell proliferation induced by R201C/G12V, indicating that oncogenic GNAS, either alone or in combination with KRASG12V promotes cell proliferation of ductal epithelia through PKA-independent mechanisms (Fig. 3E). In acinar organoids, we observed a significant ~5.2-fold and 38.7-fold increase in EdU+ cells per organoid in *KRASG12V* and *R201C/G12V*-expressing acinar structures, respectively, compared to organoids expressing R201C alone (5.7-fold) (Fig. 3F). In contrast to ductal organoids, inhibition of PKA signaling decreased the proliferation of acinar organoids, indicating that oncogenic GNAS promotes cell proliferation in a PKA-dependent manner in the acinar lineage when expressed alone or in combination with KRASG12V (Fig. 3F).

KRASG12V alone in ductal organoids did not significantly increase the total surface area of organoids but increased the percentage of organoids with visible lumen by ~5-fold (Fig. 4A, 4B, and 4C). Compared to the changes observed with R201C expression, *R201C/G12V* co-expressing ductal organoids showed a significantly reduced increase in both organoid size (8.3 Vs. 2.0 fold) and percentage of organoids with a visible lumen (5.5 Vs. 3.4 fold) (Fig. 4A, 4B and 4C). The decrease in organoid size is likely due to *KRASG12V* expression-induced multilayering and lumen filling (Fig. 4D, compare 4D” with 4H’).’ In *R201C*-expressing acinar organoids, coexpression of *KRASG12V* led to a substantial 7.8-fold increase in organoid size and a 22.7-fold increase in lumen expansion (Fig. 5A, 5B, and 5C). In comparison, KRASG12V alone produced a modest increase (~1.7-fold) in organoid size with little to no lumen expansion (Fig. 5A, 5B, 5C, 5D). The lumen expansion observed in *R201C/G12V* expressing acinar organoids is likely due to the ability of KRASG12V to induce acinar ductal metaplasia as monitored by expression of carbonic anhydrase II (CAII) (Fig. 5E), and thus creating a ductal epithelial context for GNASR201C to induce lumen expansion.

To assess whether *R201C/G12V* coexpression can generate premalignant or IPMN-like lesions in vivo, *KRASG12V*, and *R201C/G12V* expressing ductal and acinar organoids were dissociated into single cells and transplanted into the parenchyma of the mouse pancreas and allowed to grow in the presence of doxycycline for 8–14 weeks. Transplantation of *KRASG12V*-expressing ductal cells did not develop any lesions in vivo (N=4). By contrast, all four mice transplanted with KRASG12V-expressing acinar cells developed large visible tumors characterized by cellular fascicles, moderate atypia, and abundant mitosis, analogous to spindle cell neoplasm (Supplementary Fig. 2A). The differential effect of *KRASG12V* expressing ductal and acinar organoids in vivo is consistent with our previous studies, where we observed that *KRASG12D* expressing acinar organoids were more efficient in inducing adenocarcinoma-like growth compared to ductal organoids (20). Of the four mice transplanted with R201C/G12V ductal cells, two died for unknown reasons; the remaining two did not show any lesions. Among the four mice transplanted with *R201C/G12V* expressing acinar organoids, one showed lesions that did not stain positive for human nuclear antigen, suggesting a growth of unknown origin (Supplementary Fig. 2B). Together, our results suggest that *R201C/G12V* expression in both ductal and acinar structures was not sufficient to induce premalignant PanIN or IPMN-like lesions in vivo.

Establishment of long-term cultures of GNAS^{R201C} - expressing ductal organoids

We next sought to establish an *R201C* expressing ductal organoid stable culture model for pursuing mechanistic studies. While control ductal organoids did not expand beyond the first passage, *R201C*-expressing ductal organoids grown in the presence of doxycycline could be expanded for at least 15 passages (~5–6 months). Immunoblot analysis showed that *R201*C-expressing ductal organoids at later passages (P6) promoted an increase in both pPKA and pVASP, similar to that observed at the initial passage (P0), indicating that these stable cultures of R201C ductal organoids maintain their ability to activate PKA signaling (Fig. 6A). Further, stable *R201C*-expressing ductal organoids maintained their ability to induce lumen expansion and Muc2 expression (Fig. 6B, Supplementary Fig. 3A).

Next, we tested PKA-dependence by treating *R201C*-expressing ductal organoids with PKA inhibitor H89 (10uM) on different days after plating (Fig. 6C). We found that treatment of ductal organoids during the first 2 days (D0 or D2) of seeding briefly attenuated the growth of ductal organoids but maintained their ability to expand at 5.3-fold and 18.9-fold, respectively (Fig. 6D). Whereas treatment with a PKA inhibitor on Day 4 did not have any impact and the organoid growth was similar to untreated R201C-expressing organoids (Fig. 6D). Furthermore, treatment of H89 on Day 0, 2, or 4 did not affect the average percentage of Edu+ cells within each organoid (Fig. 6E), suggesting that the PKA pathway is not required for oncogenic GNAS-induced proliferation both at early and late stages of organoid growth. To rule out the long-term effects of H89 treatment, we monitored the effects of PKA inhibition within the first 24 hours of treatment. H89 inhibited PKA signaling within 24 hrs, as monitored by the reduction of p-PKA substrates and pVASP (Fig. 6F); however, this treatment did not impact the percentage of EdU+ cells/organoid (Fig. 6G and 6H). Lastly, to rule out inhibitor-specific effects, we treated R201C-expressing organoids with KT-5720 for 48 hours, another PKA inhibitor, and observed no significant effect on the percentage of Edu+ structures (Supplementary Fig. 3B, 3C, and 3D). Thus, we have established stable

cultures of R201C-expressing human ductal organoids, which retain a PKA-independent mechanism to induce cell proliferation.

Discussion

Using lineage-committed organoids, we report a surprising finding that targeted expression of mutant GNAS^{R201C} can promote the proliferation of ductal organoids through mechanisms independent of PKA signaling. By contrast, PKA signaling is required for the GNAS^{R201C}-induced proliferation of acinar organoids. Our study also demonstrates that concomitant expression of *KRAS*^{G12V} and *GNAS*^{R201C} does not enhance GNAS^{R201C}-induced proliferation or the PKA-dependence in ductal or acinar organoids. Finally, we report the feasibility of growing *GNAS*^{R201C}-expressing ductal organoids as stable cultures for at least 15 passages. These stable *GNAS*^{R201C}-expressing ductal-like organoid cultures are an ideal platform to elucidate how GNAS^{R201C} induces cell proliferation in a PKA-independent manner and identify regulators of IPMN progression.

The kinases and downstream signals that regulate oncogenic GNAS-induced proliferation are only partly understood. Although H89 is known to inhibit activities of AKT, RSK, AMPK, and ROCK (23), it does not impact our conclusion that GNAS promotes cell proliferation independent of PKA activity because H89 efficiently inhibits PKA activity. Upon activation of GNAS, increased cAMP levels predominantly activate the PKA-signaling pathway. However, previous studies indicate that increased PKA activity does not fully recapitulate the mitogenic effect of cAMP and therefore, other PKA-independent mechanisms may exist that could play a role in cAMP-dependent proliferation (24,25,26). Cyclic AMP can activate additional downstream effectors, including EPACs and cyclic nucleotide-gated ion channels (27,28,29). In this regard, our experiments indicate that treatment of organoids with Forskolin, which activates most downstream effectors of cAMP, produces more EdU+ cells than treatment with cAMP analogs that specifically activate either PKA signaling or EPAC (Supplementary Fig. 3E). Additionally, PKA mutations are not commonly observed in gastrointestinal cancers, suggesting that at least in tissues where GNAS mutations occur, GNAS may activate other targets in addition to PKA.

Previous findings indicate that cAMP activation can stimulate proliferation through PKA-independent phosphorylation of AKT, suggesting a crosstalk between the cAMP and AKT signaling (25). In addition, oncogenic GNAS modulates PI3K signaling in immortalized pancreatic ductal cell lines (30). We are in the process of conducting RNAseq and proteomics analysis to investigate if oncogenic GNAS regulates PI3K-Akt signaling to gain insights into the mechanisms by which oncogenic GNAS promotes proliferation in a PKA-independent manner.

Our results presented here demonstrate that ductal cells are more sensitive than acinar cells to oncogenic-GNAS-induced proliferation and development of cystic structures that are components of GNAS mutants expressing IPMN phenotypes in patients. In the acinar cells, oncogenic GNAS-mediated cell proliferation and cystic phenotypes are observed only in the context of oncogenic KRAS expression (Fig. 6I), suggesting that KRASG12V makes acinar cells responsive to GNASR201C. Although it is not clear how KRASG12V changes

the acinar cells, previous studies have demonstrated that activation of oncogenic KRAS (G12D) in acinar cells leads to activation of a process known as acinar to ductal metaplasia, including expression of ductal lineage regulators and markers such as SOX9 (31). Whether ductal metaplasia is necessary for oncogenic GNAS-associated phenotypes in the R201C/G12V-expressing acinar cells in the platform reported here warrants further investigation.

Concomitant mutations in KRAS/GNAS also exhibit morphological changes that are distinct from individual mutations in both ductal and acinar organoids. R201C/G12V ductal organoids appear more transformed, characterized by both large lumens and multilayering of cells within each organoid. By contrast, R201C/G12V acinar organoids have expanded lumens but no visible multilayering. Previous studies show that increased cell-type-specific cAMP production can activate ERK signaling through PKA-dependent and independent mechanisms (via EPAC-Rap1 pathway) (32,33,34). It is possible that signaling pathways downstream of GNAS-mediated activation of cAMP and KRAS-mediated activation of MAPK signaling are likely different in ductal and acinar cells. Rap1 signaling also participates in various Ras-independent functions, including regulation of cell adhesion, actin cytoskeleton, and integrin signaling (35). Further studies are needed to investigate whether morphological differences in R201C/G12V expressing ductal and acinar cells are due to cell-type specific crosstalk between cAMP and ERK signaling and differential effects of Rap1 signaling in pancreatic ductal and acinar cells.

Together, our findings validate the utility of our organoid platform to gain new insights into phenotypes associated with pre-cancerous lesions in the pancreas. Future studies aimed at identifying mechanisms by oncogenic GNAS induce proliferation of ductal cells in a PKA-independent manner and what additional genetic alterations cooperate with R201C/G12V to induce cancer progression in culture or in vivo will provide critical insights for the initiation and progression of PDAC and serve as a platform for identifying biomarkers of cancer progression.

Supplementary Material

Refer to Web version on PubMed Central for supplementary material.

Acknowledgments

We are grateful to members of the Melton laboratory for support with in vitro differentiation of stem cells, Dr. Anirban Maitra (MD Anderson) for providing us with mutant GNAS plasmids, and the members of the Muthuswamy laboratory for discussions and insights throughout the course of the project. This research was funded by an NRSA(F32) Fellowship (F32GM115201 to R.Desai)

References

1. Brosens LA, Hackeng WM, Offerhaus GJ, Hruban RH, Wood LD. Pancreatic adenocarcinoma pathology: changing “landscape”. J Gastrointest Oncol 2015;6(4):358–74. [PubMed: 26261723]
2. Sahora K, Fernández-del Castillo C. Intraductal papillary mucinous neoplasms. Curr Opin Gastroenterol 2015;31(5):424–9. [PubMed: 26125316]
3. Furukawa T, Kuboki Y, Tanji E, Yoshida S, Hatori T, Yamamoto M, et al. Whole-exome sequencing uncovers frequent GNAS mutations in intraductal papillary mucinous neoplasms of the pancreas. Sci Rep 2011;1:161. [PubMed: 22355676]

4. Wu J, Matthaei H, Maitra A, Dal Molin M, Wood LD, Eshleman JR, et al. Recurrent GNAS mutations define an unexpected pathway for pancreatic cyst development. Sci Transl Med 2011;3(92):92ra66.
5. Schönleben F, Qiu W, Remotti HE, Hohenberger W, Su GH. PIK3CA, KRAS, and BRAF mutations in intraductal papillary mucinous neoplasm/carcinoma (IPMN/C) of the pancreas. Langenbecks Arch Surg 2008;393(3):289–96. [PubMed: 18343945]
6. Yamaguchi H, Kuboki Y, Hatori T, Yamamoto M, Shiratori K, Kawamura S, et al. Somatic mutations in PIK3CA and activation of AKT in intraductal tubulopapillary neoplasms of the pancreas. Am J Surg Pathol 2011;35(12):1812–7. [PubMed: 21945955]
7. Taki K, Ohmuraya M, Tanji E, Komatsu H, Hashimoto D, Semba K, et al. GNAS(R201H) and Kras(G12D) cooperate to promote murine pancreatic tumorigenesis recapitulating human intraductal papillary mucinous neoplasm. Oncogene 2016;35: 2407–12. [PubMed: 26257060]
8. Patra KC, Kato Y, Mizukami Y, Widholz S, Boukhali M, Revenco I, et al. Mutant GNAS drives pancreatic tumourigenesis by inducing PKA-mediated SIK suppression and reprogramming lipid metabolism. Nat Cell Biol 2018;20:811–22. [PubMed: 29941929]
9. Ideno N, Yamaguchi H, Ghosh B, Gupta S, Okumura T, Steffen DJ, et al. GNAS(R201C) induces pancreatic cystic neoplasms in mice that express activated KRAS by inhibiting YAP1 signaling. Gastroenterology 2018;155:1593–607. [PubMed: 30142336]
10. Turan S, Bastepe M. GNAS Spectrum of Disorders. Curr Osteoporos Rep 2015;13(3):146–58. [PubMed: 25851935]
11. Weinstein LS, Liu J, Sakamoto A, Xie T, Chen M. Minireview: GNAS: normal and abnormal functions. Endocrinology 2004;145(12):5459–64. [PubMed: 15331575]
12. O'Hayre M, Vázquez-Prado J, Kufareva I, Stawiski EW, Handel TM, Seshagiri S, et al. The emerging mutational landscape of G proteins and G-protein-coupled receptors in cancer. Nat Rev Cancer 2013;13(6):412–24. [PubMed: 23640210]
13. Landis CA, Masters SB, Spada A, Pace AM, Bourne HR, Vallar L. GTPase inhibiting mutations activate the alpha chain of Gs and stimulate adenylyl cyclase in human pituitary tumours. Nature 1989;340(6236):692–6. [PubMed: 2549426]
14. Weinstein LS, Shenker A, Gejman PV, Merino MJ, Friedman E, Spiegel AM. Activating mutations of the stimulatory G protein in the McCune-Albright syndrome. N Engl J Med. 1991 Dec 12;325(24):1688–95. doi: 10.1056/NEJM199112123252403. [PubMed: 1944469]
15. Ramms DJ, Raimondi F, Arang N, Herberg FW, Taylor SS, Gutkind JS. Gαs-Protein Kinase A (PKA) Pathway Signalopathies: The Emerging Genetic Landscape and Therapeutic Potential of Human Diseases Driven by Aberrant Gαs-PKA Signaling. Pharmacol Rev 2021 Oct;73(4):155–197. [PubMed: 34663687]
16. Wilson CH, McIntyre RE, Arends MJ, Adams DJ. The activating mutation R201C in GNAS promotes intestinal tumourigenesis in Apc(Min/+) mice through activation of Wnt and ERK1/2 MAPK pathways. Oncogene 2010 Aug 12;29(32):4567–75. [PubMed: 20531296]
17. Matthaei H, Schulick RD, Hruban RH, Maitra A. Cystic precursors to invasive pancreatic cancer. Nat Rev Gastroenterol Hepatol 2011;8(3):141–50. [PubMed: 21383670]
18. Molin MD, Matthaei H, Wu J, Blackford A, Debeljak M, Rezaee N, et al. Clinicopathological correlates of activating GNAS mutations in intraductal papillary mucinous neoplasm (IPMN) of the pancreas. Ann Surg Oncol 2013;20(12):3802–8. [PubMed: 23846778]
19. Matthaei H, Wu J, Dal Molin M, Shi C, Perner S, Kristiansen G, et al. GNAS sequencing identifies IPMN-specific mutations in a subgroup of diminutive pancreatic cysts referred to as "incipient IPMNs". Am J Surg Pathol 2014;38(3):360–3. [PubMed: 24525507]
20. Huang L, Desai R, Conrad DN, Leite NC, Akshinthala D, Lim CM, et al. Commitment and oncogene-induced plasticity of human stem cell-derived pancreatic acinar and ductal organoids. Cell Stem Cell 2021;28(6):1090–1104. [PubMed: 33915081]
21. Leite NC, Sintov E, Meissner TB, Brehm MA, Greiner DL, Harlan DM, et al. Modeling Type 1 Diabetes In Vitro Using Human Pluripotent Stem Cells. Cell Rep 2020;32(2):107894. [PubMed: 32668238]
22. Pagliuca FW, Millman JR, Gürtler M, Segel M, Van Dervort A, Ryu JH, et al. Generation of functional human pancreatic β cells in vitro. Cell 2014;159(2):428–39. [PubMed: 25303535]

23. Limbutara K, Kelleher A, Yang CR, Raghuram V, Knepper MA. Phosphorylation Changes in Response to Kinase Inhibitor H89 in PKA-Null Cells. Sci Rep 2019;9(1):2814. [PubMed: 30808967]
24. Dremier S, Vandeput F, Zwartkruis FJ, Bos JL, Dumont JE, Maenhaut C. Activation of the small G protein Rap1 in dog thyroid cells by both cAMP-dependent and -independent pathways. Biochem Biophys Res Commun 2000;267(1):7–11. [PubMed: 10623565]
25. Cass LA, Summers SA, Prendergast GV, Backer JM, Birnbaum MJ, Meinkoth JL. Protein kinase A-dependent and -independent signaling pathways contribute to cyclic AMP-stimulated proliferation. Mol Cell Biol 1999;19(9):5882–91. [PubMed: 10454535]
26. Dremier S, Pohl V, Poteet-Smith C, Roger PP, Corbin J, Doskeland SO, et al. Activation of cyclic AMP-dependent kinase is required but may not be sufficient to mimic cyclic AMP-dependent DNA synthesis and thyroglobulin expression in dog thyroid cells. Mol Cell Biol 1997;17(11):6717–26. [PubMed: 9343436]
27. Cheng X, Ji Z, Tsalkova T, Mei F. Epac and PKA: a tale of two intracellular cAMP receptors. Acta Biochim Biophys Sin 2008;40(7):651–62. [PubMed: 18604457]
28. de Rooij J, Zwartkruis FJ, Verheijen MH, Cool RH, Nijman SM, Wittinghofer A, et al. Epac is a Rap1 guanine-nucleotide-exchange factor directly activated by cyclic AMP. Nature 1998;396:474–477. [PubMed: 9853756]
29. Kawasaki H, Springett GM, Mochizuki N, Toki S, Nakaya M, Matsuda M, et al. A family of cAMP-binding proteins that directly activate Rap1. Science 1998;282:2275–2279. [PubMed: 9856955]
30. Komatsu H, Tanji E, Sakata N, Aoki T, Motoi F, Naitoh T, et al. A GNAS mutation found in pancreatic intraductal papillary mucinous neoplasms induces drastic alterations of gene expression profiles with upregulation of mucin genes. PLoS One 2014;9(2):e87875. [PubMed: 24498386]
31. Kopp JL, von Figura G, Mayes E, Liu FF, Dubois CL, Morris JP 4th, et al. Identification of Sox9-dependent acinar-to-ductal reprogramming as the principal mechanism for initiation of pancreatic ductal adenocarcinoma. Cancer Cell 2012;22(6):737–50. [PubMed: 23201164]
32. Li Y, Dillon TJ, Takahashi M, Earley KT, Stork PJ. Protein Kinase A-independent Ras Protein Activation Cooperates with Rap1 Protein to Mediate Activation of the Extracellular Signal-regulated Kinases (ERK) by cAMP. J Biol Chem 2016;291(41):21584–21595. [PubMed: 27531745]
33. Stork PJ, Schmitt JM. Crosstalk between cAMP and MAP kinase signaling in the regulation of cell proliferation. Trends Cell Biol 2002;12(6):258–66. [PubMed: 12074885]
34. Vossler MR, Yao H, York RD, Pan MG, Rim CS, Stork PJ. cAMP activates MAP kinase and Elk-1 through a B-Raf- and Rap1-dependent pathway. Cell 1997;89(1):73–82. [PubMed: 9094716]
35. Caron E Cellular functions of the Rap1 GTP-binding protein: a pattern emerges. J Cell Sci 2003;116(Pt 3):435–40. [PubMed: 12508104]

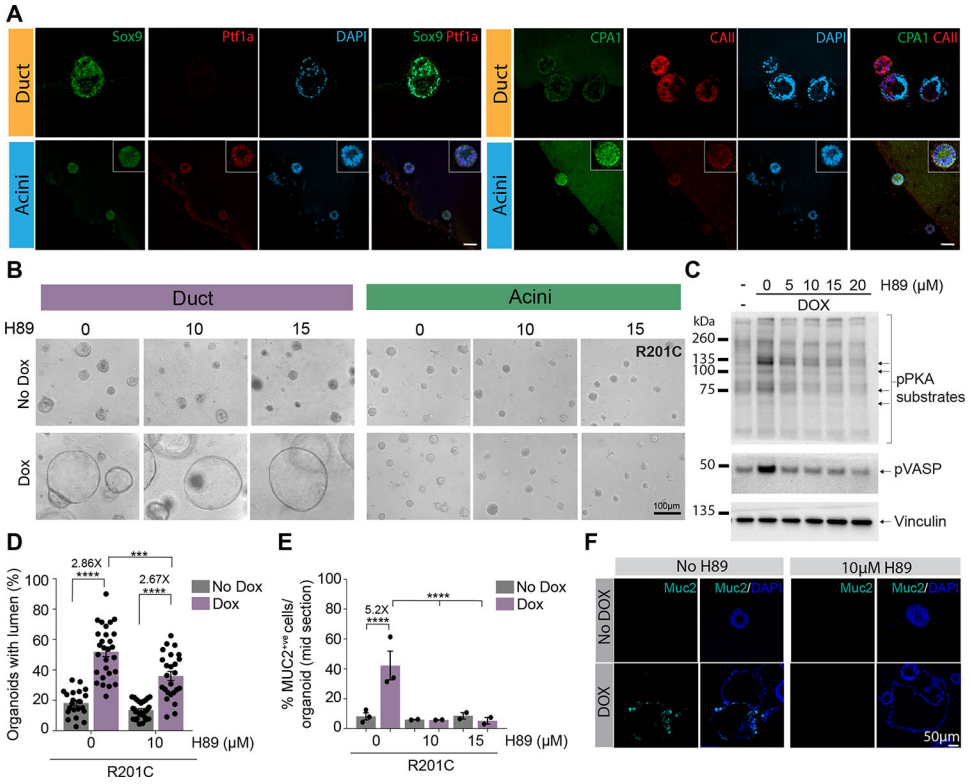

Figure 1. Oncogenic GNAS^{R201C}-expressing ductal organoids induce lumen expansion and mucin production through a PKA-dependent mechanism.

(A) Immunofluorescence staining of embryoic stem-cell pancreatic progenitor-derived ductal and acinar organoids (Day16) showing expression of ductal (Sox9 (green) and CAII(red)) and acinar (Ptf1a (red) and CPA1(green) markers. Scale bars indicate 50μm

(B) Phase Images (10X) of GNAS^{R201C}-expressing ductal and acinar organoids in the presence and absence of doxycycline with indicated doses of H89(μM) treatment. Scale bar, 100μm

(C) Western blot analysis of GNAS^{R201C}-expressing ductal organoids showing inhibition of PKA activity at different doses of H89.

(D) Percentage of GNAS^{R201C}-expressing ductal organoids with expanded lumen in the presence and absence of doxycycline, with and without H89 treatment.

(E) Percentage of GNAS^{R201C}-expressing ductal organoids with MUC2 expression in the presence and absence of doxycycline, with and without H89 treatment.

(F) Day16 R201C-expressing ductal organoids grown in the presence or absence of H89 to inhibit PKA signaling were immunostained with Muc2 (Cyan) and DAPI (blue). Scale bar indicates 50μM.

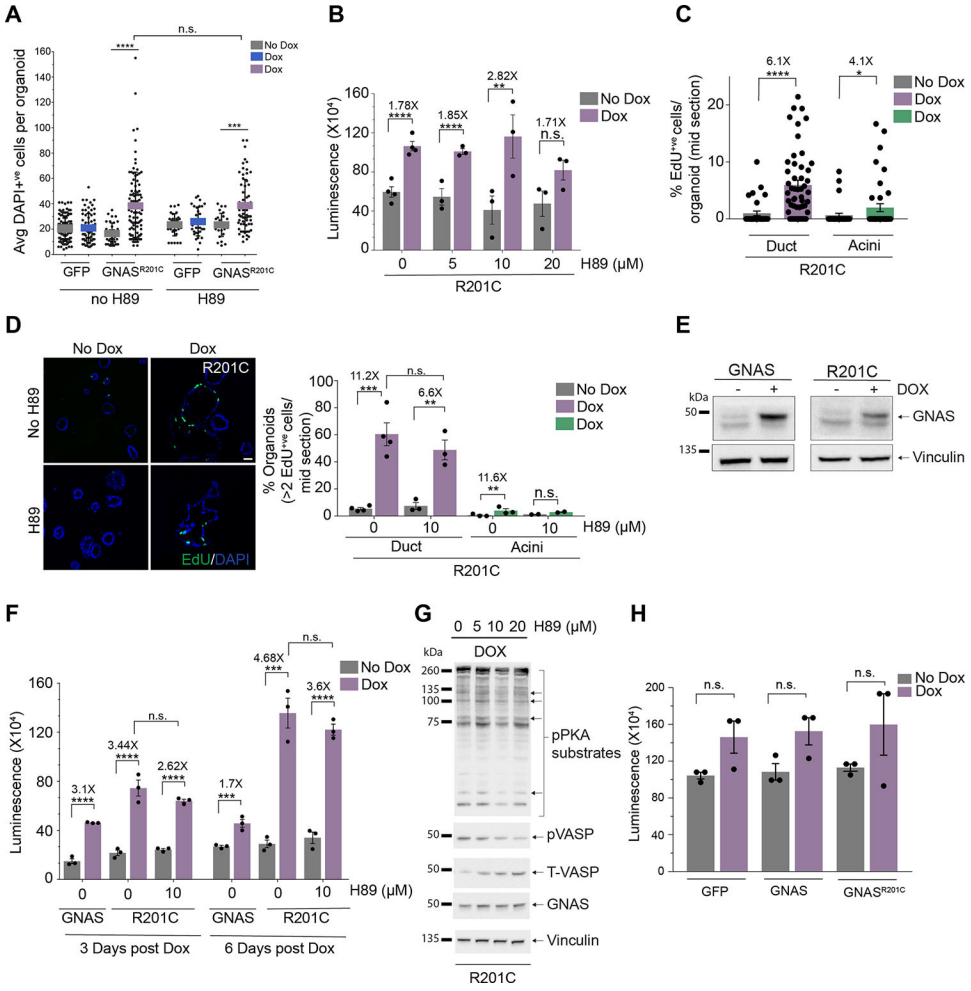

Figure 2. Oncogenic GNAS^{R201C} increases the proliferation of ductal organoids in a PKA-independent manner

(A) Scatter dot plot showing average number of DAPI^{+ve} cells per organoid in R201C-expressing ductal organoids treated with H89(10μM), N=30–100 organoids from three independent experiments. Error bar, mean±S.D

(B) Cell titer Glow Assay measuring cell viability of GNAS^{R201C}-expressing ductal organoids at different doses of H89.

(C) Percentage of EdU^{+ve} cells/organoid at the mid-plane of a Z-stack in GNAS^{R201C}-expressing ductal and acinar organoids. Mid-plane refers to the middle section of an organoid found within each histology slide section.

(D) Immunofluorescent staining of EdU^{+ve} cells in GNAS^{R201C}-expressing ductal organoids in the presence and absence of H89. Scale bar: 100μm. Bar graphs to the right represents the percentage of GNAS^{R201C}-expressing ductal and acinar organoids with at least two or more Edu^{+ve} cells at the midsection, with and without H89 treatment.

(E) Western blot analysis showing dox-inducible expression of GNAS and R201C in HPDE cells. GNAS antibody to measure GNAS protein levels. Vinculin was used as a loading control.

(F) Cell titer Glow assay measuring cell viability of Full length-GNAS (GNAS) or $GNAS^{R201C}$-expressing HPDE cells, with and without H89 treatment.
(G) Western Blot analysis showing inhibition of PKA activity in $GNAS^{R201C}$-expressing HPDE cells at multiple doses of H89, as determined by a decrease in phospho-VASP (pVASP) and a corresponding decrease in Total-VASP (T-VASP).
(H) Bar graph showing cell titer glow measurements to assess changes in cell proliferation in response to dox-inducible expression of GNAS, and R201C mutation of HPDE cells in 2D. GFP expressing cells were used a control to monitor non-specific effects, if any, of dox stimulation. Error bars represent mean±S.D, a combination of three individual experiments. n.s.(not significant)

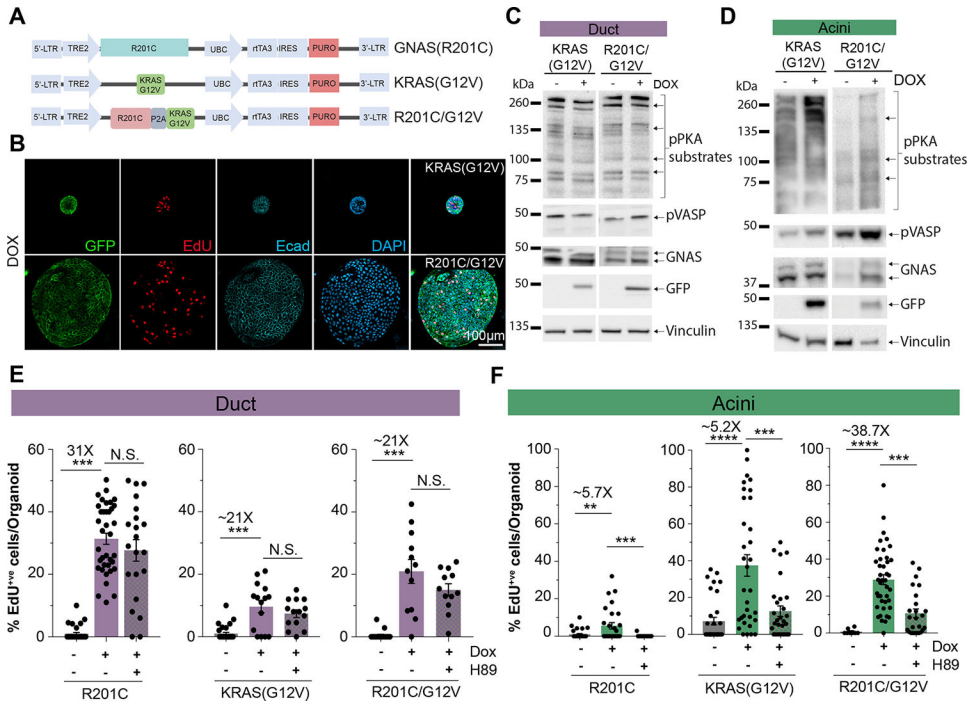

Figure 3. Co-expression of GNAS^{R201C} and KRAS^{G12V} do not cooperate in ductal and acinar organoids.

(A) Schematic of doxycycline-inducible lentiviral constructs used to express R201C, KRAS(G12V) and R201C/G12V.

(B) GFP panel (green) marks immunofluorescence images of N-terminal GFP fused KRAS(G12V) and R201C/G12V-expressing acinar organoids. EdU panel (red) marks cells that incorporated EdU, Ecadherin (membrane marker), and DAPI (nuclei) are in cyan and blue respectively.

(C and D) Western blot analysis showing PKA activity in R201C, KRAS(G12V), and R201C/G12V-expressing ductal (C) and acinar (D) organoids - as determined by total levels of phospho PKA (pPKA) substrates and phosphoVASP (pVASP). Vinculin is used as a loading control. GNAS antibody was used to measure dox-inducible changes in GNAS protein levels, and GFP immunoblots measure changes in KRASG12V protein levels.

(E and F) Percentage of EdU^{+ve} cells/organoid at the midsection in R201C, KRAS(G12V), and R201C/G12V-expressing ductal (E) and acinar (F) organoids, with and without H89 treatment. The ‘midsection’ refers to the optical section corresponding to the midplane of a z-stack, as determined during confocal imaging.

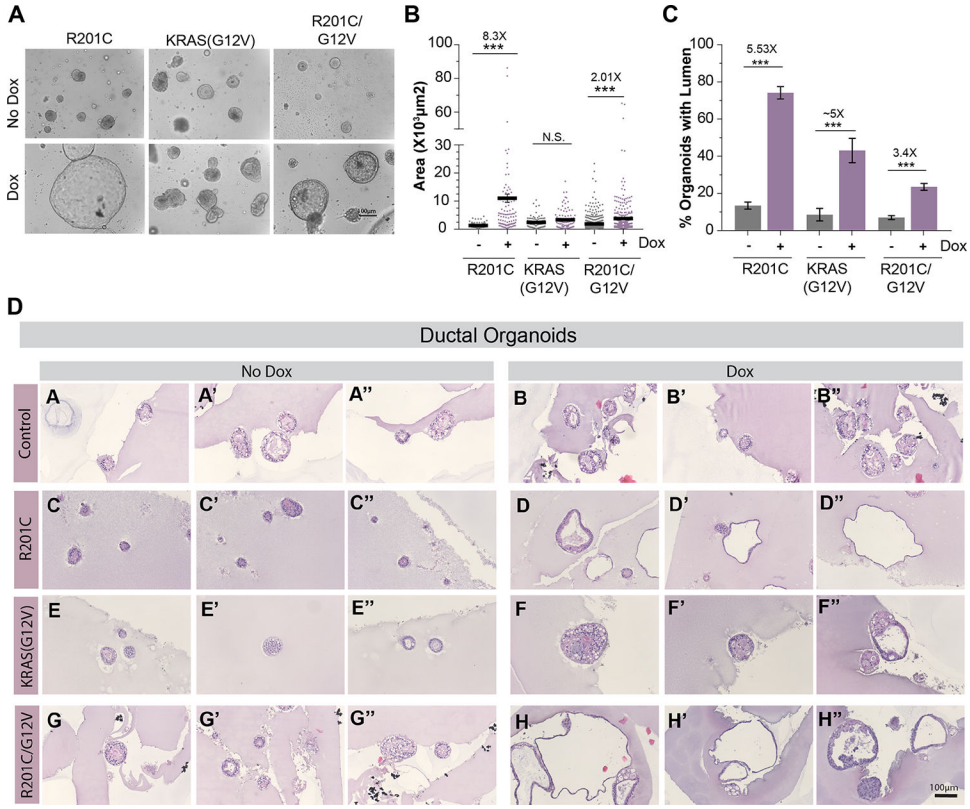

Figure 4. Co-expression of oncogenic GNAS and KRAS result in lumen filling but not lumen expansion, compared to GNAS^{R201C}-expressing ductal organoids.

(A) Phase Images (10X) of R201C, KRAS(G12V), and R201C/G12V-expressing ductal organoids in the presence and absence of doxycycline. Scale bar, 100µm

(B) Scatter dot plot showing the average total area of ductal organoids expressing GNAS^{R201C}, KRAS^{G12V}, and R201C/G12V, N=80–500 organoids, a combination of three independent experiments.

(C) Bar graph showing the average percentage of R201C, KRAS(G12V), and R201C/G12V-expressing ductal organoids with an expanded lumen in the presence and absence of doxycycline, N=80–500 organoids, a combination of three independent experiments.

(D) Histology sections of control (A-B''), R201C (C-D''), KRAS(G12V)(E-F''), and R201C/G12V(G-H'') expressing ductal organoids stained with hematoxylin and eosin. Three representative images are shown for each transgene in the absence (No Dox) and presence (Dox) of doxycycline.

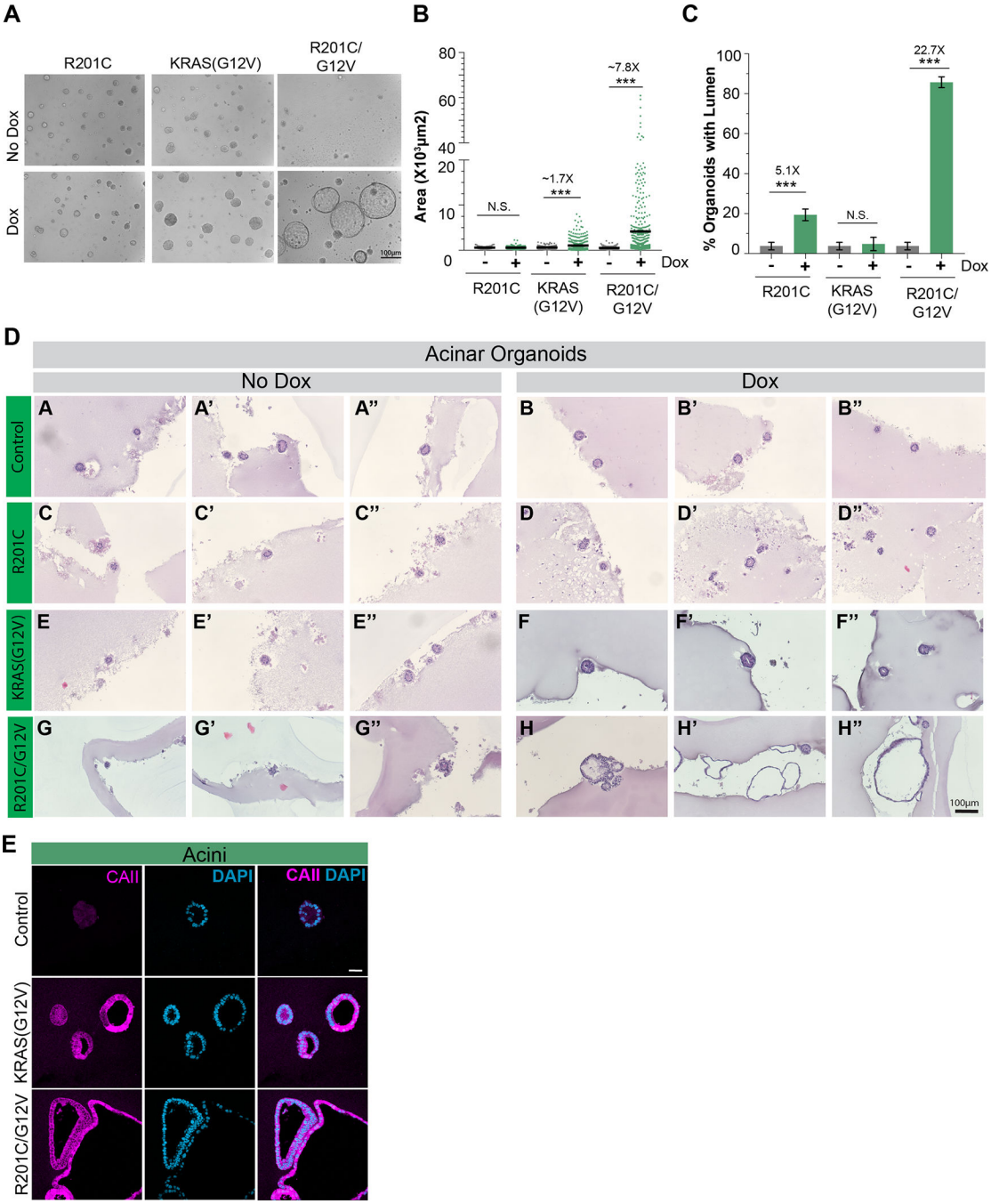

Figure 5. Co-expression of oncogenic GNAS and KRAS induces lumen expansion and ADM-like changes in acinar organoids.

(A) Phase Images (10X) of R201C, KRAS(G12V), and R201C/G12V-expressing acinar organoids in the presence and absence of doxycycline. Scale bar, 100μm

(B) Scatter dot plot showing an average total area of acinar organoids expressing R201C, KRAS(G12V), and R201C/G12V, N=80–500 organoids, a combination of three independent experiments.

(C) Bar graph showing the average percentage of R201C, KRAS(G12V), and R201C/G12V-expressing acinar organoids with an expanded lumen in the presence and absence of doxycycline, N=80–500 organoids, a combination of three independent experiments.
(D) Histology sections of control (A-B''), R201C (C-D''), KRAS(G12V)(E-F''), and R201C/G12V(G-H'') expressing acinar organoids stained with hematoxylin and eosin. Three representative images are shown for each transgene in the absence (No Dox) and presence (Dox) of doxycycline.
(E) Immunofluorescence staining of R201C/G12V-expressing pancreatic acinar organoids (Day16) showing expression of a ductal marker CAII (magenta) and DAPI (nuclei). Scale bars indicate 50μm

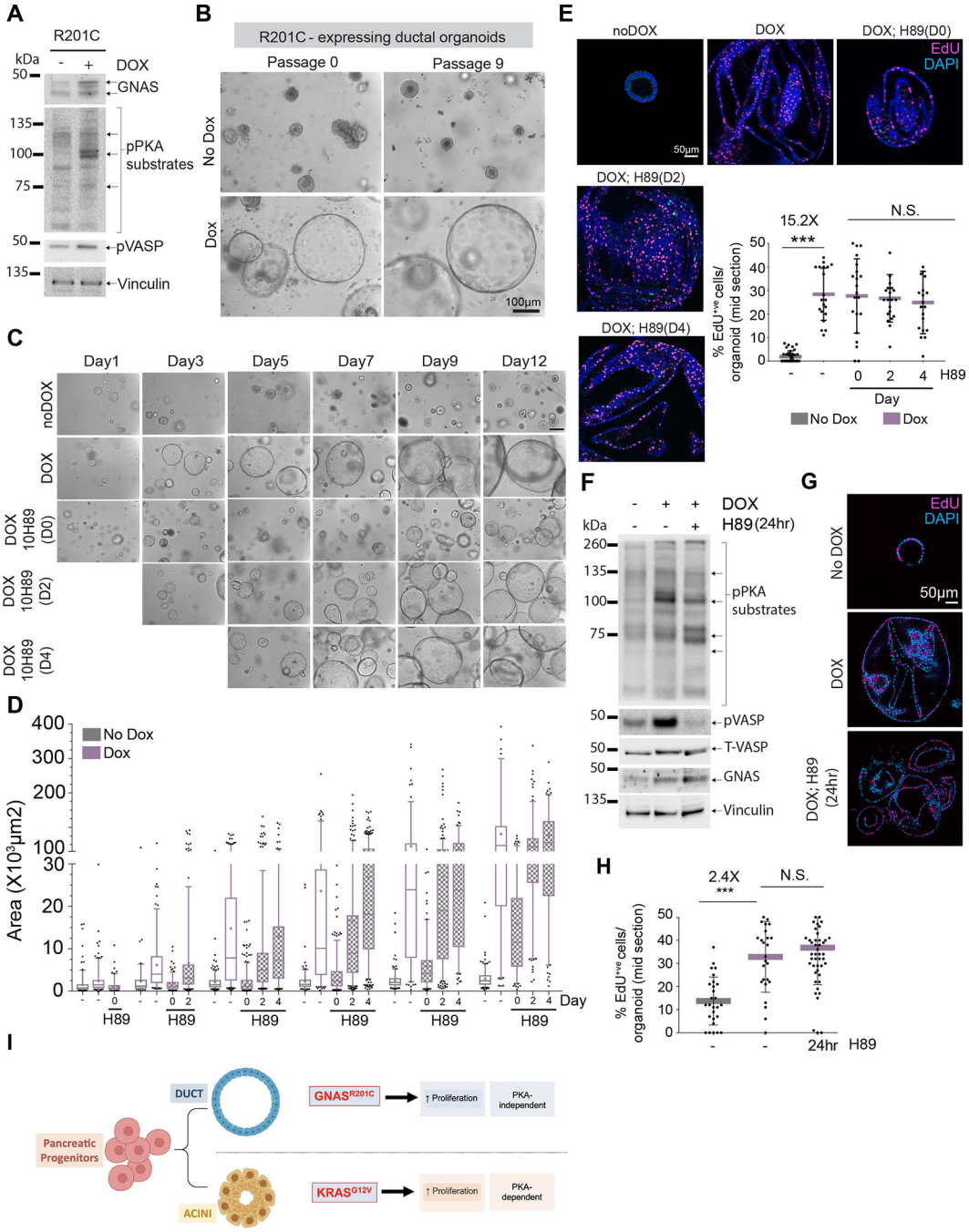

Figure 6. Characterization of stable R201C expressing ductal organoids

(A) Western blot showing activation of PKA signaling in stable R201C expressing ductal organoids.

(B) Phase images of R201C-expressing ductal organoids showing lumen expansion at multiple passages.

(C) Phase images of R201C ductal organoids treated with H89 (10µM) on Day 0 (D0), Day 2 (D2), Day 4 (D4). Doxycycline was used to express R201C from D0. Scale Bar: 100µm

(D) Box and whiskers plot showing changes in the surface area of R201C-expressing ductal organoids treated with H89 on D0, D2, and D4.
(E) Immunofluorescent images of R201C-expressing ductal organoids showing proliferative organoids labeled with EdU (red) in the presence and absence of dox (from D0), when treated with H89 from D0, D2. And D4. Scale bar, 50μm. A scatter plot shows the average percentage of Edu^{+ve} cells/organoids at the mid-plane of a Z-stack. Lines and error bars represent mean±S.D, n=3 independent experiments.
(F) Western blot showing inhibition of PKA activity after 24 hours of H89 treatment. Note: the control lane is identical to the control lane in Fig1C.
(G) Immunofluorescent images of R201C-expressing ductal organoids showing proliferative organoids labeled with EdU (red) in the presence and absence of dox (from D0) when treated with H89 for 24 hours. Scale bar, 50μm.
(H) A scatter plot shows the average percentage of Edu^{+ve} cells/organoids at the mid-plane of a Z-plane. Lines and error bars represent mean±S.D, n=3 independent experiments.
(I) A working model depicting that oncogenic GNAS acts as a dominant oncogene in ductal organoids, whereas oncogenic KRAS acts as a dominant oncogene in acinar organoids. In the context of proliferation, R201C/G12V mutations make little contribution towards R201C and KRASG12V phenotypes in ductal and acinar cells, respectively.